Journal of Catalysis **207,** 307–316 (2002)
doi:10.1006/jcat.2002.3537, available online at http://www.idealibrary.com on IDEAL®

Partial Oxidation of CH_4 over $Ni/SrTiO_3$ Catalysts Prepared by a Solid-Phase Crystallization Method

K. Takehira,[1] T. Shishido, and M. Kondo

Department of Chemistry and Chemical Engineering, Graduate School of Engineering, Hiroshima University, 1-4-1, Kagamiyama, Higashi-Hiroshima 739-8527, Japan

Received September 25, 2001; revised January 3, 2002; accepted January 21, 2002

Supported Ni catalysts on perovskite-type $CaTiO_3$, $SrTiO_3$, and $BaTiO_3$ oxides were prepared by the *solid-phase crystallization* (*spc*) method and tested for the partial oxidation of CH_4 to synthesis gas. The impregnation (*imp*) method was used for comparison. *spc*-$Ni/SrTiO_3$ showed the highest activity as well as the highest sustainability against both coke formation and reoxidation of Ni metal, followed by *spc*-$Ni/BaTiO_3$, *spc*-$Ni/CaTiO_3$, and then *imp*-$Ni/SrTiO_3$. The order of the activity was clearly confirmed in the reaction at high space velocity. Both transmission electron microscopy and temperature-programmed reduction showed the presence of finely dispersed and stable Ni metal particles on the catalysts and their amount correlated well with the order of the catalytic activity. It is suggested that incorporation of Ni is enhanced in $SrTiO_3$, followed by $BaTiO_3$, and much less in $CaTiO_3$, resulting in the higher dispersion of Ni metal particles on $SrTiO_3$. Less heat was generated over *spc*-$Ni/SrTiO_3$ during CH_4 oxidation, suggesting that the heating of the catalyst bed by CH_4 combustion must be quickly compensated for by endothermic reforming reactions. Oxygen mobility was highest over *spc*-$Ni/SrTiO_3$ as judged from CO_2 pulse measurements. The high sustainability against coke formation may be due to the high activity of finely dispersed nickel metal particles for the reforming reactions partly assisted by the mobile oxygen on the catalyst.

Key Words: **Ni catalysts; perovskite oxides; $CaTiO_3$; $SrTiO_3$; $BaTiO_3$; *in situ* reduction; high dispersion of Ni; partial oxidation of CH_4; coke formation; mobile oxygen.**

INTRODUCTION

The partial oxidation of CH_4 to synthesis gas is an established industrial process (1) which operates at high temperature (>1473 K) and under high pressure (10.1 MPa). Recently, intensive study has been done on the catalytic partial oxidation of CH_4 to synthesis gas (2–16):

$$CH_4 + 1/2O_2 \rightarrow CO + 2H_2 \quad \Delta H^0_{298K} = -36\,\text{kJ mol}^{-1}. \quad [1]$$

This process has advantages over the conventional steam reforming of CH_4 to synthesis gas, as the latter process is highly endothermic and produces synthesis gas with a H_2/CO ratio of 3. The partial oxidation of CH_4, expected to afford synthesis gas with a H_2/CO ratio of 2, makes methanol synthesis an ideal follow-up process. Ashcroft *et al.* (4–7) reported that transition metals like Ni, Ru, Rh, Pd, Ir, and Pt supported on alumina were active in this reaction at 1048 K. Especially, Ru catalyst *in situ* prepared from Ru pyrochlore ($Ln_2Ru_2O_7$) during the reaction showed a high activity (4). Ni/Al_2O_3, a typical catalyst for steam reforming, was studied for the partial oxidation of CH_4 above 973 K (10). This process involves first the oxidation of a part of CH_4 to H_2O and CO_2, followed by the reforming of CH_4 with H_2O and CO_2:

$$CH_4 + 2O_2 \rightarrow CO_2 + 2H_2O \quad \Delta H^0_{298\ K} = -801\,\text{kJ mol}^{-1} \quad [2]$$

$$CH_4 + H_2O \rightarrow CO + 3H_2 \quad \Delta H^0_{298\ K} = +206\,\text{kJ mol}^{-1} \quad [3]$$

$$CH_4 + CO_2 \rightarrow 2CO + 2H_2 \quad \Delta H^0_{298\ K} = +247\,\text{kJ mol}^{-1}. \quad [4]$$

In the partial oxidation of CH_4 to synthesis gas, coke formation over the catalyst takes place frequently, resulting in catalyst deactivation. Claridge *et al.* (7) observed that the relative rate of coke formation follows the order Ni > Pd ≫ Rh, Ru, Pt, and Ir. Nickel catalysts are highly effective for partial oxidation of CH_4 to synthesis gas, but they are unsatisfactory with respect to coke formation. We have proposed the concept of the preparation of well-dispersed and stable metal-supported catalysts, i.e., "solid-phase crystallization" (*spc*). This method has been successfully applied to the preparation of a Ni-supported catalyst for the partial oxidation of CH_4 to synthesis gas (18–24). By using $CaTiO_3$ perovskite containing small amounts of Ni in the Ti sites as the precursor, a highly dispersed and stable Ni metal was formed *in situ* on the catalyst, resulting in both high activity and sustainability against coke formation during the partial oxidation of CH_4 to synthesis gas. However, the details of the dependency of the catalytic properties on the nature of the materials have not yet been well elucidated. Here we report the relationships

[1] To whom correspondence should be addressed. Fax: 81-824-24-7744. E-mail: takehira@hiroshima-u.ac.jp.

0021-9517/02 $35.00

between the physicochemical properties and the catalytic behaviors of the Ni/perovskite catalysts prepared by the *spc* method and tested in the partial oxidation of CH_4 to synthesis gas.

EXPERIMENTAL METHODS

Preparation of the Catalyst

The *spc*-$Ni_{0.2}/CaTiO_3$, *spc*-$Ni_{0.2}/SrTiO_3$, *spc*-$Ni_{0.2}/SrTi_{0.8}O_3$, and *spc*-$Ni_{0.2}/BaTiO_3$ catalysts were obtained *in situ* by the *spc* method from the perovskite precursors prepared by the citrate method (18–24). The precursors were prepared as follows: An aqueous solution of reagent-grade nickel nitrate, alkaline earth carbonates, and titanium isopropoxide was treated with an excess amount of citric acid and ethylene glycol; this mixture was evaporated at 353–363 K to make a sol of the organometallic complex. This was followed by two-step decomposition by heating at 473 K for 5 h and 773 K for 5 h and finally by calcining at 1123 K in air for 5 h. The *imp*-$Ni_{0.2}/SrTiO_3$ catalyst was prepared by an impregnation (*imp*) method using $SrTiO_3$, which was separately prepared by the citrate method. α-Al_2O_3 and MgO were purchased and also used as supports. In both *spc* and *imp*, the Ni/Ti atomic ratio was fixed at 0.2/1.0, which corresponds to a Ni loading of 5.9 wt%. The catalyst was pressed binder-free into 25-mm-diameter pellets, using 5 tons of pressure. The pellets were calcined in air at 1173 K for 5 h and crushed to 22–30 mesh size particles.

Characterization of the Catalyst

The structures of the catalysts were studied by XRD, TEM, BET, and TPR. X-ray diffraction was measured by using a Rigaku RINT2550VHF diffractometer with Cu$K\alpha$ radiation. Transmission electron micrographs were obtained on a JEOL JEM 3000F instrument equipped with a Hitachi/Kevex H-8100/DeltaIV EDS. BET measurements were conducted using N_2 at 77 K with a BEL Japan BELSORP18 instrument. Temperature-programmed reduction of the catalyst was performed at a heating rate of 10 K min^{-1} using a mixture of 3 vol% H_2/Ar as reducing gas after passing through a 13X molecular sieve trap to remove water. A TCD was used for monitoring the H_2 consumption. Prior to the TPR measurements, the sample was calcined at 573 K for 2 h in 20 vol% O_2/N_2 gas.

Catalytic Testing

All catalysts were tested by using a temperature-programmed reaction in a mixture of $CH_4/O_2/N_2 = 10/5/20$ ml min^{-1} (all purchased from Takachiho Chemical Co. Ltd.). The reaction was carried out by increasing the reaction temperature from room temperature to 1073 K at a rate of 2.5 K min^{-1}. Moreover, the reactions for testing the coking were carried out at 1073 K for 6 h under the same conditions. A U-shaped quartz reactor was used, with the catalyst bed near the bottom. One hundred fifty milligrams of catalyst was dispersed in 2 ml of quartz beads to avoid sintering and clogging of the reactor. The hourly space velocity of the gas was changed when necessary. The thermocouple by which the reaction temperature was controlled was placed at the center of the catalyst bed. Product gases were analyzed by online gas chromatography. The selectivities to CO_2, CO, and H_2 were calculated based on the numbers of carbon and hydrogen atoms in CH_4. A blank test without the catalyst showed low enough values of 22 and 8% of O_2 and CH_4 conversion, respectively, at 1073 K. It was confirmed that no channeling of the reactant gas occurred under all experimental conditions.

After 6 h of testing, the reactor was filled with nitrogen and cooled according to normal procedures. Finally, temperature-programmed oxidation was performed by heating the reactor from room temperature to 1223 K at a rate of 2.5 K min^{-1} under air atmosphere at a flow rate of 41 ml min^{-1}. Off-gases were analyzed as usual, and the amount of coke formed on the catalyst was estimated from the amount of CO_2 formed during the reaction.

Pulse reactions were carried out to estimate the amount of mobile oxygen in the catalysts using the U-shaped quartz reactor. One hundred milligrams of the sample was treated by H_2 (1 ml × 5) pulses at 1123 K. The reduced sample was treated by a CO_2 pulse and the amount of mobile oxygen was then estimated from the amount of CO formed.

RESULTS

CH_4 Oxidation over the Catalyst

As the temperature increased from room temperature to 1073 K during the reaction, the CH_4 conversion curves clearly showed two steps (Fig. 1, left-hand side), corresponding to the combustion of CH_4 (reaction [2]) in the first step followed by reforming reactions of CH_4 to synthesis gas (reactions [3] and [4]) in the second step. The catalysts were used as prepared (after the calcination at 1123 K for 5 h) and reduced *in situ* to the active form during the reaction. The results of CH_4 oxidations over the Ni/perovskite catalysts are also shown in Table 1. The values calculated from the thermodynamic equilibrium of reactions [2], [3], and [4] are shown as references in the table. The molar ratio of $CH_4/O_2 = 2/1$ used in the reaction allowed $1/4CH_4$ to react with all O_2 to form a gas mixture of $CH_4/CO_2/H_2O$ in the combustion step (reaction [2]). The mixed gas thus formed reduces the nickel in the rest of the catalyst bed to Ni^0, which then catalyzes the reforming reaction of the remaining $3/4CH_4$ with CO_2 and H_2O at the higher temperature (reactions [3] and [4]). The combustion

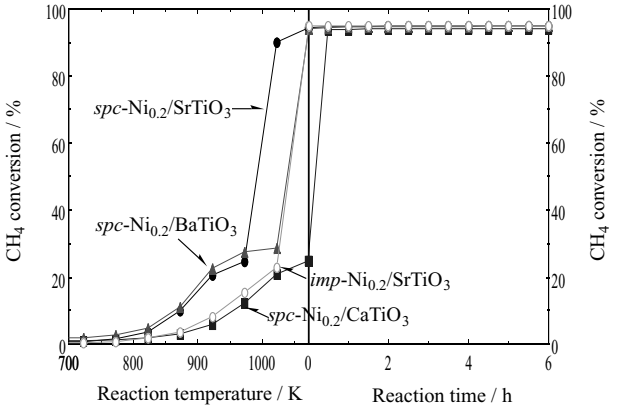

FIG. 1. Temperature-programmed oxidation of CH_4 (left-hand side) followed by life test for 6 h (right-hand side) over the Ni/perovskite catalysts.

of CH_4 took place around 25% of CH_4 conversion and was then followed by the reforming reaction to produce synthesis gas with high selectivity. A transition from combustion to reforming is clearly seen in the product distributions of each reaction, i.e., by the formation of CO_2 with high selectivity at 973 K, followed by CO and H_2 at 1073 K (Table 1). *spc*-$Ni_{0.2}/SrTiO_3$ (Fig. 1, left-hand side) showed the highest activity for both combustion and reforming, followed by *spc*-$Ni_{0.2}/BaTiO_3$ and *imp*-$Ni_{0.2}/SrTiO_3$. *spc*-$Ni_{0.2}/CaTiO_3$ showed no activity for the reforming reactions, even at 1073 K, and became active after being held under the reducing atmosphere at 1073 K for 30 min (Table 1 and Fig. 1, right-hand side).

Structure of the Ni/Perovskite Catalysts

The surface areas of the catalysts are presented in Table 2. All the catalysts showed a rather small surface area of about 10 $m^2\ g^{-1}$. The X-ray diffraction patterns of powders of *spc*-$Ni_{0.2}/CaTiO_3$, *spc*-$Ni_{0.2}/SrTiO_3$, and *spc*-$Ni_{0.2}/BaTiO_3$, together with those of *imp*-$Ni_{0.2}/SrTiO_3$, as prepared and after reaction are shown in Fig. 2. "As prepared" means "after the calcination at 1123 K for 5 h," and "after reaction" means "after temperature-programmed reaction from room temperature to 1073 K, followed by the reaction at 1073 K for 6 h." The catalysts as prepared showed the lines of the perovskite structure of $CaTiO_3$ (JCPDS: 22–153) (JCPDS: Joint Committee of Powder Diffraction Standard), $SrTiO_3$ (JCPDS: 35–734), and $BaTiO_3$ (JCPDS: 5–626), together with those of NiO (JCPDS: 4–835). Apparently only NiO was reduced to Ni metal (JCPDS: 4–850) in all the catalysts after the reaction. The intensities of the diffraction lines of each perovskite (110), NiO (111), and Ni metal (111), and the full-width at half-minimum (fwhm) values of each line are shown in Table 2. The diffraction lines of perovskite, NiO, and Ni metal were sharp and strong in the *imp* catalyst but much weaker and broader in the *spc* catalysts. Among the *spc* catalysts, the lines of NiO were observed most strongly in *spc*-$Ni_{0.2}/CaTiO_3$ (Fig. 2a), while traces of the lines were observed in both *spc*-$Ni_{0.2}/SrTiO_3$ (Fig. 2c) and *spc*-$Ni_{0.2}/BaTiO_3$ (Fig. 2e). Both the width and the strength of the line of Ni metal (Figs. 2b, 2d, and 2f) correlated well with those of the original NiO, suggesting that the order of crystal growth of both NiO and Ni metal is as follows: *spc*-$Ni_{0.2}/CaTiO_3$ > *spc*-$Ni_{0.2}/BaTiO_3 \geq$ *spc*-$Ni_{0.2}/SrTiO_3$.

TABLE 1

CH_4 Oxidation over the Ni/Perovskite Catalysts[a]

Catalyst	Conversion (%)		Selectivity (%)		
	CH_4	O_2	CO	H_2	CO_2
spc-$Ni_{0.2}/CaTiO_3$	24.8	100	0	1.4	100
	93.8[b]	100	98.3	98.2	1.7
spc-$Ni_{0.2}/SrTiO_3$	94.4	100	97.9	97.9	2.1
spc-$Ni_{0.2}/BaTiO_3$	93.9	100	96.5	95.9	3.5
imp-$Ni_{0.2}/SrTiO_3$	94.7	100	97.8	97.8	2.2
thermodynamics[c]	(97.1)	(100)	(96.8)	(97.0)	(3.2)

[a] Catalyst, 150 mg; $CH_4/O_2/N_2$ = 10/5/20 ml min^{-1}; temperature, 1073 K.

[b] After reaction at 1073 K for 30 min.

[c] Numbers in parentheses show the values calculated from thermodynamic equilibrium of reactions [2]–[4].

The results of the TEM observation of the catalysts after the reactions for 6 h are shown in Fig. 3. *imp*-$Ni_{0.2}/SrTiO_3$ showed large Ni metal particles, with a diameter of around 40–50 nm, and aggregates of perovskite single crystals (Fig. 3a). In *spc*-$Ni_{0.2}/CaTiO_3$, the size of the Ni metal particles decreased to about 20–30 nm, and in addition several dark spots appeared on the perovskite single crystals (Fig. 3b). The number of dark spots increased with a further decrease in the size of the Ni metal particles to less than 20 nm on *spc*-$Ni_{0.2}/BaTiO_3$ (Fig. 3c). Some substructures were observed and were probably due to the orientation of the crystal growth of the perovskite in this catalyst. No Ni metal particles were observed, and the number of the dark spots increased enormously on *spc*-$Ni_{0.2}/SrTiO_3$ (Fig. 3d). However, the presence of XRD lines due to Ni metal (Fig. 2) suggests that the Ni metal particles still exist in *spc*-$Ni_{0.2}/SrTiO_3$. The size and the shape of the dark spots are not clear enough, and therefore their quantitative evaluation is not possible. In a previous paper (22), it was shown that the TEM image of *spc*-Ni/$BaTiO_3$ under high magnification suggests that the dark spots may be the aggregates of finely dispersed Ni metal particles with a diameter of less than 1 nm. This strongly suggests that ultrafine particles of Ni metal were formed on the present catalysts prepared by the *spc* method. We failed to determine the distribution of the Ni metal particles by H_2 adsorption, suggesting that either the size of the Ni metal particles was too small or their nature was changed by the interaction with the supports. According to the TEM results, the relative amounts of ultrafinely dispersed Ni metal

TABLE 2

Surface Areas and X-Ray Diffraction Data of the Ni/Perovskite Catalysts

Catalyst	Surface area ($m^2\ g^{-1}$)	Perovskite (110) intensity[a]		NiO (111)		Ni (111)	
		Before[b]	After[c]	Intensity[a]	fwhm[d]	Intensity[a]	fwhm[d]
spc-$Ni_{0.2}/CaTiO_3$	10.3	3067	1779	261	0.34	299	0.32
spc-$Ni_{0.2}/SrTiO_3$	12.4	9138	5279	219	0.54	135	0.43
spc-$Ni_{0.2}/BaTiO_3$	13.7	4305	4000	80	0.50	133	0.30
imp-$Ni_{0.2}/SrTiO_3$	12.8	8691	11227	367	0.26	467	0.14

[a] cps.
[b] Before the reaction.
[c] After the reaction.
[d] Full width at half minimum.

in the total surface Ni metal can be placed in the following order: *spc*-$Ni_{0.2}/SrTiO_3$ > *spc*-$Ni_{0.2}/BaTiO_3$ > *spc*-$Ni_{0.2}/CaTiO_3$ > *imp*-$Ni_{0.2}/SrTiO_3$. Generally, finely dispersed metal particles are not very stable and tend to sinter. However, this is not the case in the present catalysts, since ultrafinely dispersed Ni metal particles were still observed after the reaction for 50 h at 1073 K on *spc*-$Ni_{0.2}/SrTiO_3$ and *their activity did not decline* at all during the reaction. This may be due to a strong interaction between the Ni metal particles and the perovskite support, since the Ni species were originally incorporated in the crystal structure in the precursor.

Stability of the Catalysts

After the steady state of reforming activity was attained on all the catalysts at 1073 K, the temperature of the reactor was decreased step by step, and the reaction was carried out for 2 h at each temperature (Fig. 4). *spc*-$Ni_{0.2}/CaTiO_3$, *spc*-$Ni_{0.2}/SrTiO_3$, and *spc*-$Ni_{0.2}/BaTiO_3$ showed a reforming activity which almost followed thermodynamic equilibrium, while only *imp*-$Ni_{0.2}/SrTiO_3$ showed a decrease in reforming activity when temperature decreased below 873 K. The activity of *spc*-$Ni_{0.2}/CaTiO_3$ was not stable, and the conversions of CH_4 and O_2 decreased from 39 to 9% and from 100 to 36%, respectively, during the reaction at 773 K for 2 h. During the CH_4 oxidation over *spc*-$Ni_{0.2}/CaTiO_3$ at 773 K, the reaction slowly changed from the reforming mode to the combustion mode judging from the product selectivities and the CH_4/O_2 conversions. Both *spc*-$Ni_{0.2}/SrTiO_3$ and *spc*-$Ni_{0.2}/BaTiO_3$ still produced CO and H_2 together with CO_2 following thermodynamic equilibrium, while both *imp*-$Ni_{0.2}/SrTiO_3$ and *spc*-$Ni_{0.2}/CaTiO_3$ produced only CO_2. This may be due to the surface oxidation of Ni metal over the catalyst. In the XRD patterns of *imp*-$Ni_{0.2}/SrTiO_3$ and *spc*-$Ni_{0.2}/SrTiO_3$ after the reaction at 573 K for 2 h, i.e., by further decreasing the temperature, the peaks of NiO were observed more strongly in *imp*-$Ni_{0.2}/SrTiO_3$ than in *spc*-$Ni_{0.2}/SrTiO_3$. These results suggest that Ni metal particles are more easily oxidized on the former than on the latter. *spc*-$Ni_{0.2}/CaTiO_3$ also showed peaks of NiO more enhanced than those of *spc*-$Ni_{0.2}/SrTiO_3$. Thus, it is likely that Ni metal species formed on both *imp*-$Ni_{0.2}/SrTiO_3$ and *spc*-$Ni_{0.2}/CaTiO_3$ are not stable and are quickly oxidized on the former and slowly on the latter in the presence of O_2.

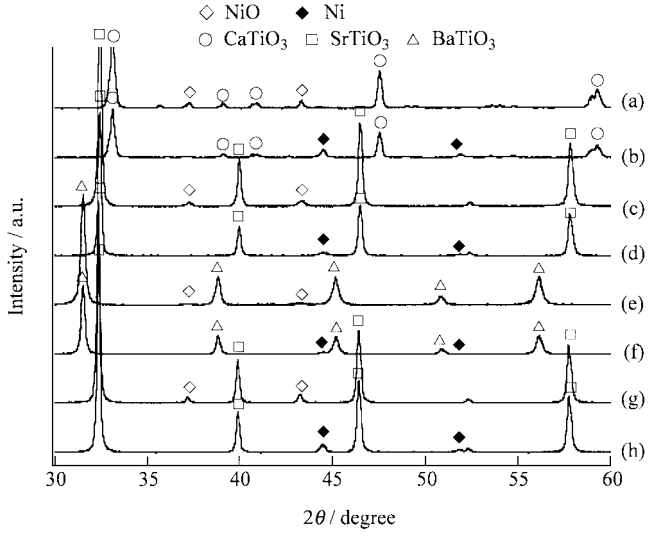

FIG. 2. X-ray diffraction patterns of the Ni/perovskite catalysts. (a) *spc*-$Ni_{0.2}/CaTiO_3$ as prepared, (b) *spc*-$Ni_{0.2}/CaTiO_3$ after reaction, (c) *spc*-$Ni_{0.2}/SrTiO_3$ as prepared, (d) *spc*-$Ni_{0.2}/SrTiO_3$ after reaction, (e) *spc*-$Ni_{0.2}/BaTiO_3$ as prepared, (f) *spc*-$Ni_{0.2}/BaTiO_3$ after reaction, (g) *imp*-$Ni_{0.2}/SrTiO_3$ as prepared, and (h) *imp*-$Ni_{0.2}/SrTiO_3$ after reaction.

Effect of the Space Velocity

As seen in Table 1, the reactions are almost controlled by the thermodynamic equilibrium at 1073 K, and the comparison of the activities between the Ni/perovskite catalysts is not easy. The activities can be rationally compared under kinetically controlled conditions, and the reaction was therefore carried out at 1073 K by increasing the space velocity (Fig. 5). The CH_4 conversion decreased significantly

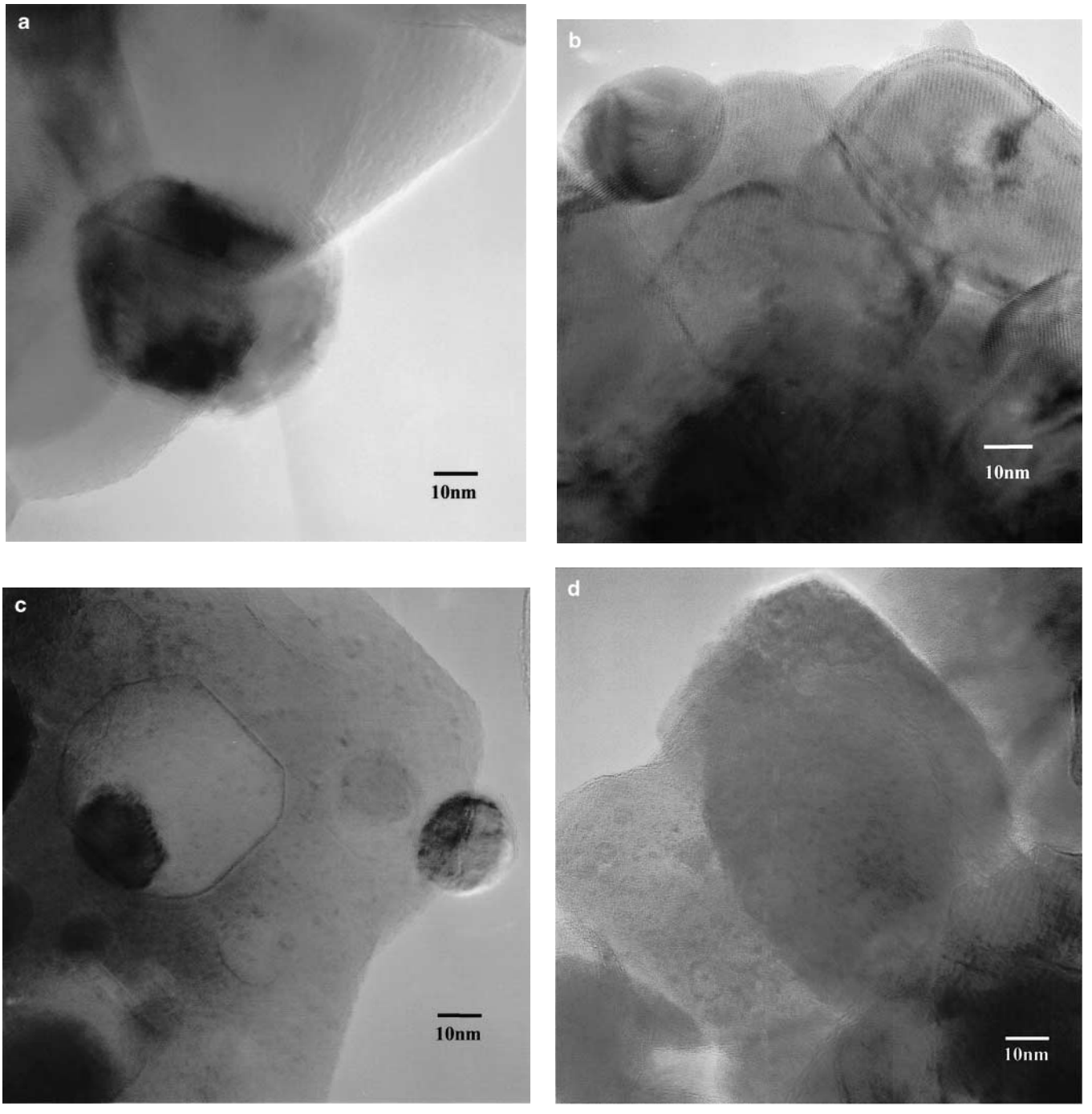

FIG. 3. TEM observations of the Ni/perovskite catalysts after reaction. (a) *imp*-$Ni_{0.2}/SrTiO_3$, (b) *spc*-$Ni_{0.2}/CaTiO_3$, (c) *spc*-$Ni_{0.2}/BaTiO_3$, and (d) *spc*-$Ni_{0.2}/SrTiO_3$.

with increasing space velocity on *imp*-$Ni_{0.2}/SrTiO_3$, while the *spc*-catalysts, among which *spc*-$Ni_{0.2}/SrTiO_3$ showed the highest activity followed by *spc*-$Ni_{0.2}/BaTiO_3$ and *spc*-$Ni_{0.2}/CaTiO_3$, were active enough even under the high space velocity. The order of the activity shown by the CH_4 conversion at high space velocity correlated well with that of the CO selectivity (Fig. 5) as well as with that of the H_2 selectivity, suggesting that ultrafinely dispersed Ni metal particles are effective for the partial oxidation of CH_4 into synthesis gas. At increasing space velocity, a large amount of CH_4 is oxidized (reaction [1]) and the heat is accumulated in the catalyst bed, resulting in an increase in the temperature. This may also cause a shift in the thermodynamic equilibrium to increase the selectivity of CO. In the present work,

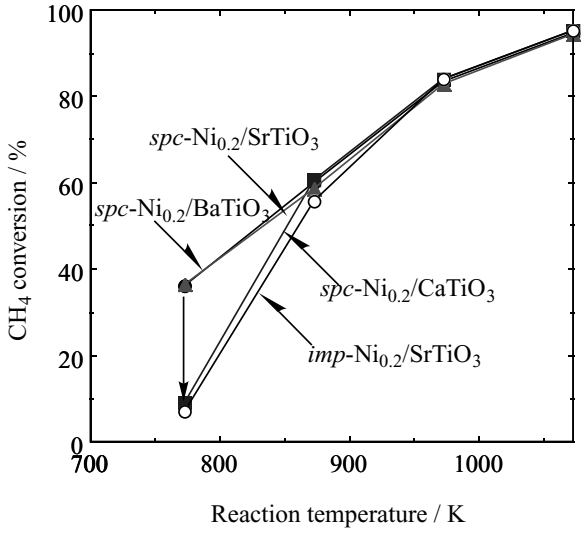

FIG. 4. Oxidation of CH_4 over the Ni/perovskite catalysts by stepwise decrease of the reaction temperature from 1073 to 773 K.

however, the reaction temperature was controlled and always kept at 1073 K at the center of the catalyst bed, even at high space velocity. The heat of the reaction, if it appeared, was almost compensated by lowering the temperature of the electric furnace. Moreover, the heat of exothermic combustion was also effectively compensated by the following endothermic reforming reactions (*vide infra*). When the CO_2 reforming of CH_4 was carried out on the same catalysts, the selectivity of CO settled down in the same order as that for the catalytic activity. These results strongly suggest that the effect of temperature can be neglected and that the CO selectivity reflects the character of the catalysts well. Thus, *spc*-$Ni_{0.2}/SrTiO_3$ was the most effective catalyst for the production of synthesis gas and maintained a high activity as well as a high selectivity to CO above 98%, even at the high space velocity of 112,000 ml g-cat^{-1} h^{-1}.

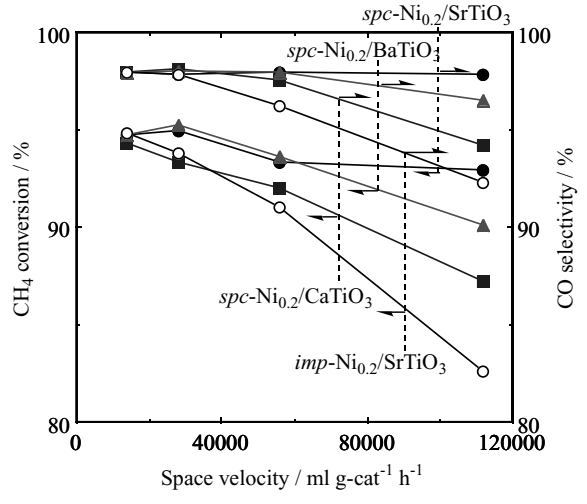

FIG. 5. Effect of the space velocity on CH_4 conversion and CO selectivity in the CH_4 oxidation over the Ni/perovskite catalysts.

Coke Formation and Mobile Oxygen on the Catalyst

The amount of coke formed on the catalyst after the reaction for 6 h was measured. *imp*-$Ni_{0.2}/SrTiO_3$ showed the highest value (4.7 wt%) of coke formation. Among the *spc*-catalysts, both *spc*-$Ni_{0.2}/SrTiO_3$ (0.22 wt%) and *spc*-$Ni_{0.2}/BaTiO_3$ (0.32 wt%) showed smaller amounts of coke formation, while *spc*-$Ni_{0.2}/CaTiO_3$ afforded the largest amount (4.0 wt%) of coke after the reaction. It is reported that finely dispersed Ni metal particles are effective for sustainability against coke formation (17). However, we did not observe a clear difference in anti-coking properties between *spc*-$Ni_{0.2}/SrTiO_3$ and *imp*-$Ni_{0.2}/SrTiO_3$ in the CH_4 pyrolysis at 1073 K (25). At 1073 K and at atmospheric pressure, the main source of coke formation is considered to come from CH_4 pyrolysis rather than from CO disproportionation (7). Both catalysts quickly lost the activities of CH_4 pyrolysis, since Ni metal particles were encapsulated in graphite layers on both *spc*-$Ni_{0.2}/SrTiO_3$ and *imp*-$Ni_{0.2}/SrTiO_3$. Quick deposition of carbon on the Ni surface exceeded the migration of carbon over the surface of or through the bulk of Ni metal particles, resulting in the deactivation of the catalysts. A quick elimination of carbon formed on the catalyst surface will be effective for keeping the catalyst active, and this may be achieved by the highly active sites for the reforming reactions. Thus, the high dispersion alone cannot explain the anti-coking property of the catalyst well.

We have reported that a mobile oxygen species is effective for lowering the coking on the Ni catalyst (21). The amount of mobile oxygen in the supports or the catalysts was measured by the CO_2 pulse reaction. The samples of both supports and catalysts were treated with H_2 pulses. The mobile oxygen in the samples reacted with H_2 to form H_2O and oxygen vacancies, which were in turn reoxidized with CO_2 to form CO. The amounts of CO formed during 10 CO_2 pulses on several samples are shown in Fig. 6. Thus, the amounts of mobile oxygen in the supports and the catalysts were calculated from the CO integrated during the pulse experiments (Table 3). Generally, the perovskite supports showed higher values than those for the conventional supports, among which the values for $SrTiO_3$ were higher than those of $CaTiO_3$ and $BaTiO_3$. When Ni was supported on $SrTiO_3$, a significant increase was observed on *spc*-$Ni_{0.2}/SrTiO_3$, while no substantial change was observed on *imp*-$Ni_{0.2}/SrTiO_3$. This is probably due to the incorporation of Ni in the Ti site in $SrTiO_3$. A similar increase was observed when Ni was supported on MgO but not so clearly on α-Al_2O_3. This may reflect that Ni forms a solid solution in MgO (26) but not in α-Al_2O_3.

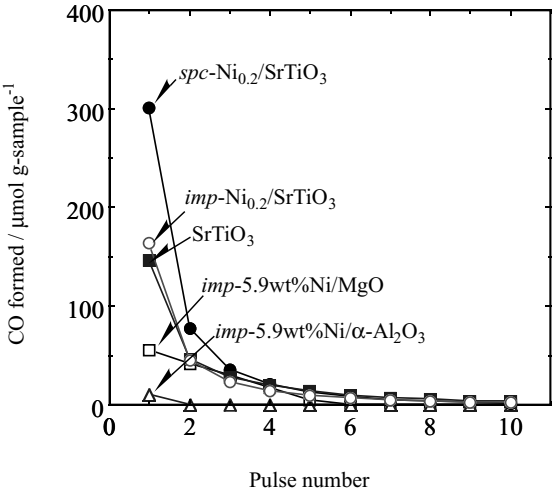

FIG. 6. CO_2 pulse reaction on the catalysts and the supports.

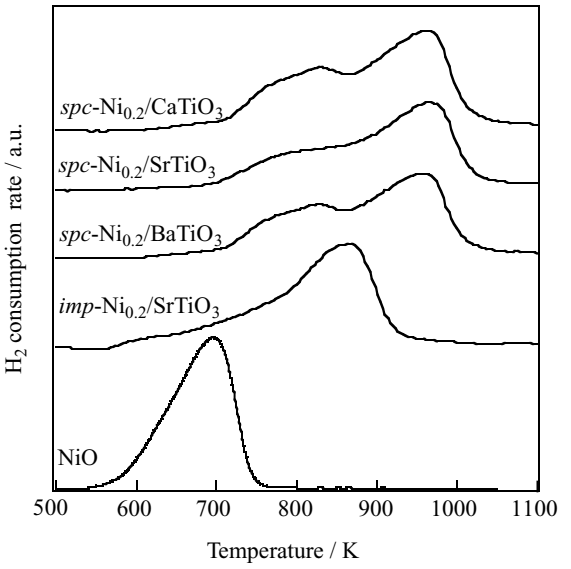

FIG. 7. TPR of the Ni/perovskite catalysts.

The order of the oxygen mobility of the supports and the catalysts almost coincides with that of the sustainability against coking, suggesting that mobile oxygen may be effective for eliminating coke formed on the catalyst surface. The oxygen species can migrate from the support to the surface of the Ni metal particles by reverse spillover and react with the carbon species formed from either CH_4 or CO. Oxygen vacancies can be refilled by oxygen species from either O_2 or CO_2. Fine Ni metal particles may have an advantage in the carbon removal, since the path of oxygen migration to carbon species is rather short compared to that of large-sized Ni metal particles. It is likely that a synergic effect between the fine Ni metal particles and the oxygen mobility explains the sustainability against coking on the *spc*-catalysts.

TPR of the Ni/Perovskite Catalysts

Ni species originally included in the crystal structure of the perovskite precursors may appear at the surface of the catalyst during the reaction. During the TPO (Fig. 1), the reducibility of Ni species substantially changed depending on the nature of the catalyst. Moreover, TEM and XRD observations suggest that the surface Ni dispersion strongly depends on both the preparation method and the nature of the support. TPR of the catalysts was carried out under H_2 gas flow (Fig. 7). NiO showed the reduction peak to Ni metal at around 690 K. When NiO was loaded on the perovskite, the peak of the Ni reduction shifted to a higher temperature; this temperature was lower for *imp*-$Ni_{0.2}/SrTiO_3$ than for *spc*-catalysts. Ni loading by the *imp* method resulted in the formation of large NiO particles on the perovskite, and the TPR revealed a rather simple reduction of NiO at low temperature. The *spc*-catalysts showed two peaks of the Ni reduction, i.e., a broad one between 800 and 850 K and a relatively sharp one at around 960 K, the former corresponding to the peak observed on *imp*-$Ni_{0.2}/SrTiO_3$. The intensities of the former peaks were in the order *spc*-$Ni_{0.2}/CaTiO_3$ > *spc*-$Ni_{0.2}/BaTiO_3$ > *spc*-$Ni_{0.2}/SrTiO_3$, coinciding well with the order of the peak intensity of NiO in the XRD of these catalysts (Table 2). This suggests that NiO particles formed by the phase separation during the *spc* preparation were loaded on the surface of perovskite and were reduced at 800–850 K. The second peak, which appeared around 960 K, differed from the broad peak, and was observed at 968, 960, and 958 K for *spc*-$Ni_{0.2}/SrTiO_3$, *spc*-$Ni_{0.2}/BaTiO_3$, and *spc*-$Ni_{0.2}/CaTiO_3$, respectively. Again the reducibility of Ni species was in the order of *spc*-$Ni_{0.2}/CaTiO_3$ > *spc*-$Ni_{0.2}/BaTiO_3$ > *spc*-$Ni_{0.2}/SrTiO_3$, suggesting that the second peak was due to the reduction of Ni species incorporated in the perovskite structure.

TABLE 3

Oxygen Mobility of the Supports and the Catalysts[a]

Sample	Amount of mobile oxygen (μmol g-sample^{-1})
$CaTiO_3$	143
$SrTiO_3$	285
$BaTiO_3$	76.4
MgO	4.0
α-Al_2O_3	0.7
spc-$Ni_{0.2}/SrTiO_3$	468
imp-$Ni_{0.2}/SrTiO_3$	277
imp-Ni/MgO	148
imp-Ni/α-Al_2O_3	11.0

[a] Amount of mobile oxygen was measured by CO_2 pulse reactions.

DISCUSSION

During the partial oxidation of CH_4, the combustion reaction is a necessary first step not only for affording CO_2 and H_2O but also for reducing the Ni species; the reduction can be accelerated in the absence of oxygen and make Ni species active for the reforming reactions. The appearance of the reforming activities on *spc*-$Ni_{0.2}/CaTiO_3$ was slow compared to that of those on *spc*-$Ni_{0.2}/BaTiO_3$ and *spc*-$Ni_{0.2}/SrTiO_3$; nonetheless, Ni species in *spc*-$Ni_{0.2}/CaTiO_3$ can be more easily reduced than those in the other catalysts, as observed in TPR results (Fig. 7). This may be due to the low activity of *spc*-$Ni_{0.2}/CaTiO_3$ for the CH_4 combustion (Fig. 1) resulting in a slow reduction of the catalyst system. In contrast, the most sustainable precursor against reduction, i.e., *spc*-$Ni_{0.2}/SrTiO_3$, was accompanied by an early appearance of reforming activity; this may be due to a high combustion activity (Fig. 1). *imp*-$Ni_{0.2}/SrTiO_3$ showed a low activity for CH_4 combustion and an easy reduction of the surface nickel species, resulting in an activity in between that of *spc*-$Ni_{0.2}/SrTiO_3$ and that of *spc*-$Ni_{0.2}/CaTiO_3$.

The CH_4 combustion (reaction [2]) is exothermic, while the reforming reactions of CH_4 by H_2O and CO_2 (reactions [3] and [4]) are endothermic. The former is rapid over the conventional Ni-supported catalysts, while the latter is slow, resulting in the formation of a hot spot at the beginning of the catalyst bed (10). Moreover, an increasing space velocity may result in an enormous increase in the temperature due to an accumulation of the heat of combustion. In the present work, the reaction temperature was controlled at the center of the catalyst bed, and therefore the temperature of the furnace had to be lowered at high space velocity. Actually, the temperature of the outer wall of the reactor was measured and compared to that of the catalyst bed. The differences between the center of the catalyst bed and the outer wall of the reactor in the temperatures observed at a space velocity of 14,000 ml h^{-1} g-cat^{-1} were −12, −4, and −9 K for *spc*-$Ni_{0.2}/CaTiO_3$, *spc*-$Ni_{0.2}/SrTiO_3$, and *spc*-$Ni_{0.2}/BaTiO_3$, respectively. Those for the *imp*-catalysts supported on the perovskites, including *imp*-Ni/MgO and *imp*-Ni/α-Al_2O_3, were between −20 and −30 K. Moreover, the temperature distribution was measured by using either 200 or 400 mg of the catalyst without diluting with quartz beads to see the temperature profile more precisely (Table 4). The temperature differences between the top and the bottom of the catalyst bed were 5–6 and 17 K for *spc*-$Ni_{0.2}/SrTiO_3$ and *imp*-$Ni_{0.2}/SrTiO_3$, respectively. Combustion occurs at the top of the catalyst bed, resulting in increasing temperature, while reforming at the center and at the bottom causes decreasing temperature. Even though it is not easy to measure the temperature at the hot spot, smaller values of overheating were observed over the *spc*-catalysts than over the *imp*-catalysts, among which the smallest value was obtained over *spc*-$Ni_{0.2}/SrTiO_3$. This value most likely reflects the high activity of *spc*-$Ni_{0.2}/SrTiO_3$ in the reforming reactions [3] and [4]; the heat formed by exothermic combustion (reaction [2]) is quickly removed by the endothermic reforming reactions [3] and [4], resulting in the small increase in temperature. In contrast, the low activity of the *imp*-catalysts for the reforming reactions cannot eliminate the heat, resulting in both heat accumulation and a large difference in temperatures.

TABLE 4

Temperature Profile in the Catalyst Bed[a]

Catalyst	CH_4 conv. (%)	Temperature in catalyst bed (K)		
		Head	Center	Tail
spc-$Ni_{0.2}/SrTiO_3$[b]	95.2	1084	1081	1079
spc-$Ni_{0.2}/SrTiO_3$[c]	94.6	1081	1076	1075
imp-$Ni_{0.2}/SrTiO_3$[d]	89.5	1095	1088	1078

Note. Reaction temperature was controlled at outer wall of the reactor at 1073 K.

[a] $CH_4/O_2/N_2 = 10/5/20$ ml min^{-1}. Catalyst, 200[b,d] and 400[c] mg. The length of the catalyst bed, 4.5[b] and 8.0[c,d] mm.

Tolerance factors [$t = (r_A + r_O)/\sqrt{2}(r_B + r_O)$, where r_A, r_B, and r_O are ionic radii of A, B, and O, respectively, in ABO_3 perovskite] were calculated for each perovskite precursor. $CaTiO_3$ and $BaTiO_3$ have values of 0.966 and 1.06 and orthorhombic and tetragonal structures, respectively (27). $SrTiO_3$ has the ideal value of 1.00 and has the most stable cubic crystal structure (28). The traces of NiO peaks observed in the XRD patterns of both *spc*-$Ni_{0.2}/SrTiO_3$ and *spc*-$Ni_{0.2}/BaTiO_3$ may be due to either a good solubility of Ni in the perovskite or, at least, crystallites too small to give a signal. After catalytic testing, the XRD patterns of *spc*-$Ni_{0.2}/SrTiO_3$ and *spc*-$Ni_{0.2}/BaTiO_3$ also showed traces of Ni metal peaks. We believe that a substantial part of the nickel in the structure was reduced to its metallic form on the surface during the reaction. The nickel metal particles are probably too small to give reasonable signals in XRD.

From the intensities and fwhm of the strongest lines of each perovskite (110), NiO (111), and Ni metal (111) (Table 3), it is concluded that $SrTiO_3$ crystallized well in both *spc*-$Ni_{0.2}/SrTiO_3$ and *imp*-$Ni_{0.2}/SrTiO_3$, followed by $BaTiO_3$ in *spc*-$Ni_{0.2}/BaTiO_3$ and then $CaTiO_3$ in *spc*-$Ni_{0.2}/CaTiO_3$. It is obvious from the change in the perovskite (110) intensity that the crystallinity of $SrTiO_3$ decreased in *spc*-$Ni_{0.2}/SrTiO_3$ during the reaction, while no significant change was observed in *imp*-$Ni_{0.2}/SrTiO_3$, suggesting that Ni in the perovskite structure was released in the former catalyst during the reaction. The NiO (111) peak was weakened in the order of *imp*-$Ni_{0.2}/SrTiO_3$ > *spc*-$Ni_{0.2}/CaTiO_3$ > *spc*-$Ni_{0.2}/SrTiO_3$ > *spc*-$Ni_{0.2}/BaTiO_3$, and the Ni metal (111) peak also decreased in the same order. The linewidth of the NiO (111) peak was the largest for *spc*-$Ni_{0.2}/SrTiO_3$, followed by *spc*-$Ni_{0.2}/BaTiO_3$,

spc-$Ni_{0.2}/CaTiO_3$, and then *spc*-$Ni_{0.2}/SrTiO_3$; that of the Ni metal (111) peak was of the same order. All nickel species must be segregated from the perovskite structure in the case of *imp*-$Ni_{0.2}/SrTiO_3$, considering the preparation method of impregnation. All the *spc*-catalysts showed smaller peak intensities of NiO (111) and larger linewidths of Ni metal (111) than those of *imp*-$Ni_{0.2}/SrTiO_3$. This suggests that the segregation of Ni species in the *spc*-catalysts was less significant than that in *imp*-$Ni_{0.2}/SrTiO_3$. A substantial amount of Ni species must either be incorporated into the perovskite structure or, at least, exist as finely dispersed particles that cannot be detected by XRD.

Iwahara *et al.* (29) reported that the solid solution formation range is limited to $x = 0.1$ or less in $CaTi_{1-x}Ni_xO_{3-\delta}$. We failed to detect evidence for Ni incorporation by a shift of the diffraction lines of *spc*-$Ni_{0.2}/SrTiO_3$. This may be due to the amount of Ni incorporation, being too small. The driving force of the Ni migration from the perovskite lattice to the surface may be partly due to the thermodynamic equilibrium in the structure. The amount of oxygen defects (δ) in $SrTi_{1-x}Ni_xO_{3-\delta}$ prepared under an oxygen-rich atmosphere can be increased under the reducing atmosphere. The increase in δ may be accompanied by the reduction of metal cations in the structure. The reduction of Ni^{2+} (or even Ni^{3+}) to Ni^0 may be much easier than that of Ti^{4+} to Ti^{3+}, even when the thermodynamic equilibria between NiO/Ni and TiO_2/Ti_4O_7 are compared (30). Ni^0 formed by the reduction can no longer stay in the oxide lattice, resulting in the migration to and deposition on the surface. Thus, Ni may appear on the surface during the reaction to form highly dispersed metal species.

CONCLUSION

The *spc*-$Ni_{0.2}/CaTiO_3$, *spc*-$Ni_{0.2}/SrTiO_3$, and *spc*-$Ni_{0.2}/BaTiO_3$ catalysts were prepared *in situ* during the reaction from the perovskite-type mixed-oxide precursors and tested for the partial oxidation of CH_4 to synthesis gas. *spc*-$Ni_{0.2}/SrTiO_3$, followed by *spc*-$Ni_{0.2}/BaTiO_3$ and *spc*-$Ni_{0.2}/CaTiO_3$, showed the highest activity as well as the highest sustainability against coking on the catalyst; *spc*-$Ni_{0.2}/SrTiO_3$ also showed stable activity even under oxidizing atmosphere. The incorporation of Ni was most enhanced in $SrTiO_3$, followed by $BaTiO_3$, and much less in $CaTiO_3$, resulting in a higher dispersion of Ni metal particles on the former support. These results coincided well with the order of the activity at high space velocity *spc*-$Ni_{0.2}/SrTiO_3$ > *spc*-$Ni_{0.2}/BaTiO_3$ > *spc*-$Ni_{0.2}/CaTiO_3$. The reaction proceeds by CH_4 combustion followed by reforming of CH_4 with H_2O and CO_2, and the heat of combustion is quickly removed by the reforming on the highly active catalyst. The high and stable activity may be due to highly dispersed and stable Ni metal particles on the perovskite. The high sustainability against coke formation may be due to the high activity for the reforming reactions partly assisted by the mobile oxygen in the perovskite supports.

ACKNOWLEDGMENTS

The financial support of both the New Energy and Industrial Technology Development Organization and the Hiroshima Industrial Technology Organization is warmly acknowledged. Thanks are due to Mr. E. Tanabe of the Hiroshima Prefectural Institute of Industrial Science and Technology for the TEM measurements.

REFERENCES

1. Mandelik, R. G., Newsome, D. S., and Kellogg, P., *in* "Encyclopedia of Chemical Technology" (R. E. Kirk and D. F. Othmer, Eds.), 3rd edition, Vol. 12, p. 938. Wiley–Interscience, New York, 1980.
2. Pena, M. A., Gomez, J. P., and Fierro, J. L. G., *Appl. Catal. A* **144**, 7 (1996).
3. Armor, J. N., *Appl. Catal. A* **176**, 159 (1999).
4. Ashcroft, A. T., Cheetham, A. K., Foord, J. S., Green, M. L. H., Grey, C. P., Murrell, A. J., and Vernon, P. D. F., *Nature* **344**, 319 (1990).
5. Vernon, P. D. F., Green, M. L. H., Cheetham, A. K., and Ashcroft, A. T., *Catal. Lett.* **6**, 181 (1990).
6. Jones, R. H., Ashcroft, A. T., Waller, D., Cheetham, A. K., and Thomas, J. M., *Catal. Lett.* **8**, 169 (1991).
7. Claridge, J. B., Green, M. L. H., Tsang, S. C., York, A. P. E., Ashcroft, A. T., and Battle, P. D., *Catal. Lett.* **22**, 299 (1993).
8. Hickman, D. A., and Schmidt, L. D., *Science* **259**, 343 (1993).
9. Choudhary, V. R., Rajput, A. M., and Prabhakar, B., *J. Catal.* **139**, 326 (1993).
10. Dissanayake, D., Rosynek, M. P., Kharas, K. C. C., and Lunsford, J. H., *J. Catal.* **132**, 117 (1991).
11. Dissanayake, D., Rosynek, M. P., and Lunsford, J. H., *J. Phys. Chem.* **97**, 3644 (1993).
12. Nakamura, J., Kubushiro, K., and Uchijima, T., *Stud. Surf. Sci. Catal.* **77**, 373 (1993).
13. Nakagawa, K., Ikenaga, N., Teng, Y., Kobayashi, T., and Suzuki, T., *J. Catal.* **186**, 405 (1999).
14. Basini, L., Guarinoni, A., and Aragno, A., *J. Catal.* **190**, 284 (2000).
15. Sato, K., Nakamura, J., Uchijima, T., Hayakawa, T., Hamakawa, S., Tsunoda, T., and Takehira, K., *J. Chem. Soc., Faraday Trans.* **91**, 1655 (1995).
16. Basile, F., Basini, L., D'Amore, M., Fornasari, G., Guarinoni, A., Matteuzzi, D., Del Pierro, G., Trifiro, F., and Vaccari, A., *J. Catal.* **173**, 247 (1998).
17. Bartholomew, C. H., *Catal. Rev.–Sci. Eng.* **24**, 67 (1982).
18. Andersen, A. G., Hayakawa, T., Tsunoda, T., Orita, H., Shimizu, M., and Takehira, K., *Catal. Lett.* **18**, 37 (1993).
19. Takehira, K., Hayakawa, T., Harihara, H., Andersen, A. G., Suzuki, K., and Shimizu, M., *Catal. Today* **24**, 237 (1995).
20. Hayakawa, T., Harihara, H., Andersen, A. G., York, A. P. E., Suzuki, K., Yasuda, H., and Takehira, K., *Angew. Chem. Int. Ed. Engl.* **35**, 192 (1996).
21. Hayakawa, T., Harihara, H., Andersen, A. G., Suzuki, K., Yasuda, H., Tsunoda, T., Hamakawa, S., York, A. P. E., Yoon, Y. S., Shimizu, M., and Takehira, K., *Appl. Catal. A* **149**, 391 (1997).

22. Shiozaki, R., Andersen, A. G., Hayakawa, T., Hamakawa, S., Suzuki, K., Shimizu, M., and Takehira, K., *J. Chem. Soc., Faraday Trans.* **93**, 3225 (1997).
23. Hayakawa, T., Suzuki, S., Nakamura, J., Uchijima, T., Hamakawa, S., Suzuki, K., Shishido, T., and Takehira, K., *Appl. Catal. A* **183**, 273 (1999).
24. Takehira, K., Shishido, T., and Kondo, M., *Shokubai* **42**, 354 (2000).
25. Jia, J., Tanabe, E., Wang, P., Ito, K., Morioka, H., Wang, Y., Shishido, T., and Takehira, K., *Catal. Lett.* **76**, 183 (2001).
26. Arena, F., Frusteri, F., Parmaliana, A., Plyasova, L., and Schmakov, A. N., *J. Chem. Soc., Faraday Trans.* **92**, 469 (1996).
27. Kay H. F., and Bailey, P. C., *Acta Crystallogr.* **10**, 219 (1957).
28. Ceh, M., Kolar, D., and Golic, L., *J. Solid State Chem.* **68**, 68 (1987).
29. Iwahara, H., Esaka, T., and Mangahara, T., *J. Appl. Electrochem.* **18**, 173 (1988).
30. "Denki Kagaku Binran," The Electrochemical Society of Japan, p. 129. Maruzen, Tokyo, 1988.